Disorder-dominated and Scattering-dominated Thermal Transport in Clathrate Hydrates

Iyyappa Rajan Panneerselvam[1], Haoran Cui[1], Theodore Maranets[1], Yan Wang[1]

Department of Mechanical Engineering, University of Nevada, Reno, Reno, NV 89557

Abstract

Methane hydrate (MH) is an ice-like compound where methane molecules are encased within a lattice of water molecules. Found abundantly on ocean floors, MHs can influence future methane supplies, ocean floor stability, and climate change. In this study, a high-precision deep neural network interatomic potential for MHs is developed using ab initio molecular dynamics. Our findings reveal a transition between disorder-dominated and scattering-dominated lattice thermal transport in partially filled MHs, which are the most common form in real-world conditions. Although guest methane molecules have a minimal effect on the anharmonicity of the host lattice and the phonon band structure, they significantly increase the scattering rate of host lattice phonons by enlarging their anharmonic scattering phase space. Spectral phonon analysis further shows that methane guest molecules scatter low-frequency phonons associated with water molecule vibrations, considerably reducing the thermal conductivity of filled MHs.

Keywords: Clathrate hydrate, Phonon, Thermal conductivity, Disorder, Scattering

*Corresponding author
Email address: yanwang@unr.edu (Yan Wang)
[1]Since 1880.

1. Introduction

Clathrate hydrates (CH), commonly known as gas hydrates, constitute a unique class of nonstoichiometric compounds wherein water molecules form hydrogen-bonded cages that encapsulate hydrocarbon guest molecules. These crystalline structures emerge under conditions of high pressure and low temperature, predominantly within the deep-sea floor and Arctic permafrost regions. The remarkable ability of these compounds to trap and condense gas molecules, particularly methane, leading to the formation of methane hydrates (MH), underscores their substantial potential as a revolutionary energy resource [1, 2]. However, the extraction of MH poses significant environmental challenges, including concerns related to climate change, marine landslides, and the potential for oil and gas flowline accidents resulting from unwanted hydrate decomposition. Achieving a comprehensive understanding of the response of MH, and CH in general, to changing thermal environments during production or climate change necessitates a thorough understanding of their thermal transport properties.

Previous thermal measurements of CHs [3, 4, 5, 6, 7, 8] have generally demonstrated low and weakly temperature-dependent thermal conductivity (κ), resembling a glass-like behavior, in contrast to ice. A crucial disparity between ice and CH crystals lies in the presence of guest molecules in the latter, as shown in Fig. 1a-d for the unit cells and supercells of filled and hollow MHs. While one might intuitively expect guest molecules to enhance κ by occupying the otherwise hollow water cages in CHs, theoretical calculations have predicted that κ of filled CHs can be lower than that of their hollow counterparts [9, 10]. Various mechanisms have been proposed to elucidate this intriguing phenomenon, which is not unique to CHs but also observed in other inorganic clathrate materials [4, 11, 12, 9, 13, 10]. A prominent theory attributes this phenomenon to the scattering of host lattice phonons by guest molecules or atoms trapped within the cages [4, 11]. Furthermore, studies report that guests in clathrates can increase the anharmonicity of the host lattice [9], flatten acoustic phonon

branches [12], expand anharmonic phonon scattering phase space [9, 10], or localize propagating phonons [14], all contributing to the reduced κ observed in filled CHs. These intricate and occasionally contradictory effects of guest molecules on thermal transport in CHs necessitate a meticulous, case-by-case examination.

Experimental investigations of the thermal transport properties of CHs are challenged by the demanding conditions and intricate apparatus required for the extraction, transportation, maintenance, and measurement of CH samples, especially those of pure and pristine quality. The inherent complexities in maintaining sample quality may contribute to variations in κ data obtained from diverse experiments. A notable defect involves the absence of guest molecules in specific cages, resulting in partially filled CHs with structural disorder—indeed, the prevalent form of CHs in nature. Recent studies have revealed that structural disorder can diminish the κ of covalent crystals by suppressing coherent phonons [15, 16, 17, 18, 19], which typically serve as the primary heat carriers in complex materials. However, understanding how structural disorder precisely affects thermal transport in intricate molecular crystals like CHs remains elusive.

Given the challenges in experimentally probing the thermal transport properties of CHs, atomistic simulations, particularly molecular dynamics (MD) simulations, provide a promising avenue for exploration. However, the precision of traditional empirical interatomic potentials in MD simulations has been constrained. Although earlier MD studies on CHs using conventional potentials have contributed to our comprehension of specific facets of thermal transport physics, this current work strives for a more profound investigation by harnessing high-precision deep neural network interatomic potentials, thereby mitigating the limitations of previous research. As shown in Figs. 1e and f, our DNN potential attains an outstanding energy accuracy on the order of 1×10^{-5} eV/atom and a force accuracy on the order of 1×10^{-2} eV/$\mathring{A}$.

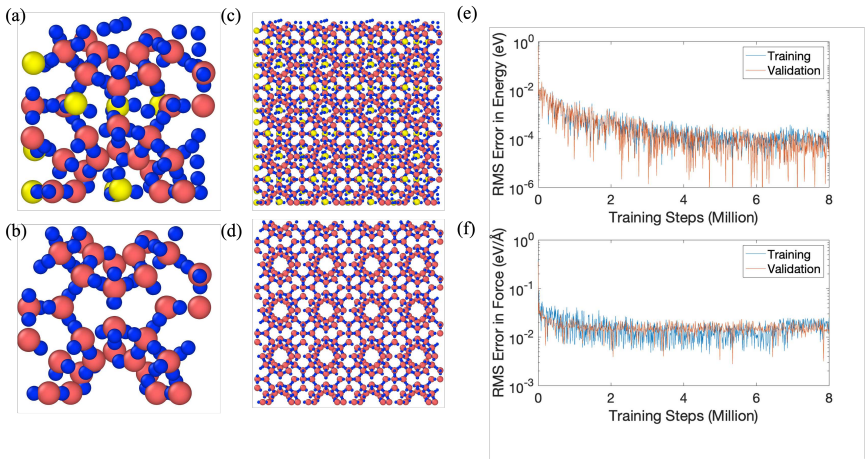

Figure 1: (a) and (b) The atomic structure of the unit cell of (a) filled MH and (b) hollow MH. (c) and (d) Representative 4×4×4 supercells of (c) filled MH and (d) hollow MH. (e) and (f) Training and validation statistics of the deep neural network potential for MH, displaying high accuracy in energy and force predictions.

2. Methodology

2.1. Development of deep neural network (DNN) interatomic potential

First, we perform ab initio molecular dynamics (AIMD) simulations using the Vienna ab initio simulation package (VASP) [20, 21] for a type-I methane hydrate (MH) unit cell with dimensions $11.62\mathring{A} \times 11.62\mathring{A} \times 11.62\mathring{A}$. The AIMD simulations utilize a Γ-centered scheme, employing a plane-wave cut-off energy of 600 eV, a Gaussian smearing width of 0.05 eV, and a convergence threshold of 10^{-8} eV for self-consistent electronic iteration, ensuring precise force calculations. Within the NVT ensemble, simulations are carried out at temperatures of 273 K, 298 K, and 300 K, each consisting of 10,000 steps. Additionally, simulations within the NPT ensemble are conducted at temperatures of 273 K and 298 K, with applied pressures ranging from 0 to 1.0 GPa. The resultant data, including instantaneous lattice vectors, atomic trajectories, atomic forces, and system energies, are employed to train a DNN interatomic potential using the DeePMD-kit package [22, 23]. The training process incorporates the full relative coordinates to construct the descriptor, employing a cutoff radius of 6.0 $\mathring{A}$ along

with the smoothing cutoff radius of 0.5 $\mathring{A}$. The embedding net comprises 3 hidden layers with 25, 50, and 100 neurons, respectively, while the fitting net consists of 3 hidden layers, each containing 240 neurons. The initial learning rate, decay steps, and decay rate are set at 0.001, 8 million, and 3.51×10^{-8}, respectively.In the Supplementary Materials, we provide the DNN model file of the interatomic potential trained in this work.

2.2. Equilibrium Molecular Dynamics (EMD)

We conduct EMD simulations using the LAMMPS package [24]. A $4\times4\times4$ supercell of type-I MH is employed to compute κ. The simulation employs a small time step size of 0.05 fs, and the Nos'e-Hoover [25, 26] thermostat and barostat are applied to relax the structure at the target temperature and 1,000 bars, each for a minimum of 50 ps. Subsequently, the simulation transitions to plain time integration for 750 ps, during which we record system heat fluxes [27], eventually converting them to κ based on the Green-Kubo formalism [28, 29].

2.3. Nonequilibrium molecular dynamics (NEMD)

In NEMD, an MH supercell of length L and a cross-sectional area of 4 by 4 unit cells is positioned between hot and cold baths, each spanning a length of 16.2$\mathring{A}$. After a similar structural relaxation process as our EMD simulations, atoms within the 7$\mathring{A}$ layer at both ends of the system are frozen, mimicking a fixed boundary condition. Subsequently, the simulation is switched to plain time integration in LAMMPS, where Langevin thermostats [30] maintain the temperatures of the hot and cold baths at $1.1\times$ and $0.9\times$ the target temperature, respectively. This process extends for 800 ps to ensure the establishment of a steady-state heat transfer. The apparent κ of the MH supercell, which depends on L, is determined from the steady-state heat current and temperature gradient based on Fourier's law [31], mimicking experimental measurements.

2.4. Spectral energy density (SED) analysis

SED quantifies the kinetic energy of a phonon mode. It is defined on the time-domain normal mode coordinates, $q_{k,v}(t)$, as [32, 33]

$$q_{\boldsymbol{k},v}(t) = \sum_{\alpha}^{3} \sum_{b}^{n} \sum_{l}^{N_c} \sqrt{\frac{m_b}{N_c}} u_{\alpha}^{l,b}(t) e_{b,\alpha}^{\boldsymbol{k},v*} exp[i\boldsymbol{k} \cdot \boldsymbol{r}_0^l], \tag{1}$$

where $u_{\alpha}^{l,b}(t)$ represents the αth component of the displacement of bth basis atom in the lth unit cell, m_b is atomic mass, N_c is the total number of primitive unit cells of the entire system, t is time, $\boldsymbol{k}$ denotes wave vector, v is phonon polarization, and $\boldsymbol{r}_0$ is the equilibrium position of each unit cell. $q_{\boldsymbol{k},v}(t)$ data are collected from EMD in the NVE ensemble for 400 ps, ensuring a high resolution of 0.0025 THz for analyzing phonon properties in the frequency domain. Subsequently, SED is calculated through Fourier transform ($\mathcal{F}[\cdot]$) of the time derivative of $q_{\boldsymbol{k},v}(t)$ as

$$\Phi_{\boldsymbol{k},v}(\omega) = |\mathcal{F}[\dot{q}_{\boldsymbol{k},v}(t)]|^2 = \frac{C_{\boldsymbol{k},v}}{(\omega - \omega_{\boldsymbol{k},v}^A)^2 + (\tau_{\boldsymbol{k},v}^{-1})^2/4}, \tag{2}$$

where $\Phi_{\boldsymbol{k},v}(\omega)$ is the SED, ω is the angular frequency, and C is a constant. The transformed data (the SED peaks in Fig. 5) is fitted with the Lorentzian function to obtain the peak position $\omega_{\boldsymbol{k},v}^A$ and phonon lifetime ($\tau_{\boldsymbol{k},v}$).

3. Results and Discussion

Figure 2a illustrates the temperature-dependent κ of hollow, 50% filled, and 100% filled MH obtained from equilibrium MD (EMD) simulations. Across all three filling ratios, κ consistently decreases as the temperature rises from 50K to 200K, aligning well with the anticipated trend dictated by the anharmonic Umpklapp scattering mechanism [34].

Notably, as depicted in Fig. 2a, the κ of hollow MHs consistently surpasses that of their 100% filled counterparts. While this observation may initially appear inconsistent with classical heat transfer expectations, which would suggest an increase in κ for a porous material with decreasing porosity, it is crucial to

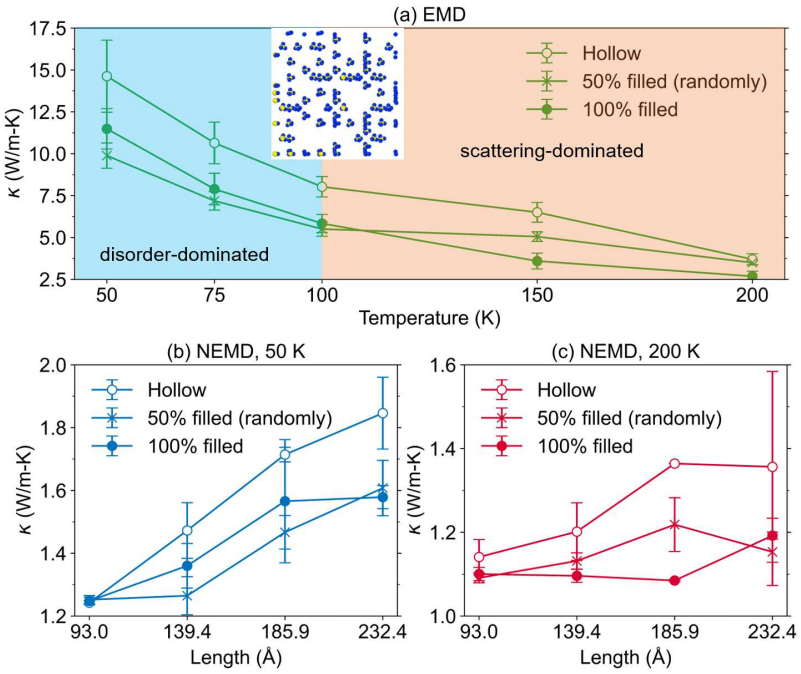

Figure 2: Lattice thermal conductivity κ of hollow, 50% (random) filled, and 100% filled MHs predicted by EMD and NEMD simulations. (a) Temperature-dependent κ predicted by EMD. The inset shows the positions of guest methane molecules inside the 50% filled MH structure, where yellow and blue circles denote carbon and hydrogen atoms, respectively. Three different 50% filled MH structures, each with randomly positioned guest molecules, are used to predict the κ values at 50 K and 200 K, to better account for the randomness in 50% filled structures. (b) and (c) Length-dependent κ predicted by NEMD simulations at 50 K and 200 K, respectively.

recognize the multifaceted roles undertaken by guest molecules as fillers. Firstly, filling the originally hollow host lattice reduces porosity, potentially leading to an increase in κ. Secondly, guest molecules introduce phonon scattering within the host lattice through phenomena like"rattling" [11, 13] or resonance scattering [35], well-known mechanisms for reducing κ in clathrate structures. Thirdly, guest molecules can reduce κ of CHs by increasing the anharmonicity of the host lattice [9, 36, 10]. Fourth, they can reduce κ by flattening phonon bands via "avoided crossing" [12]. These mechanisms, where the first increases κ while the remaining three reduce it, offer valuable insights into the potential impacts of guest molecules on κ of MHs. The subsequent sections of this paper will meticulously analyze the specific roles played by methane guest molecules.

A prominent observation in Fig. 2a, which, to our best knowledge, was never reported, is the intersection of the κ-temperature curves of 50% filled MH and 100% filled MH. Specifically, the κ of 50% filled MH is lower than that of 100% filled MH at temperatures below 100 K, while at temperatures above 100 K, the 50% filled MH exhibits a higher κ than the 100% filled MH.

Taking into account the previously discussed negative effects on κ induced by guest molecules, one would reasonably anticipate that the κ of 50% filled MH surpasses that of the 100% filled counterpart, given the former's reduced number of guest molecules available to scatter phonons, increase anharmonicity, or flatten phonon bands. Our EMD data, as illustrated in Fig. 2a for the above-100 K range, corroborates this expectation by revealing a monotonically decreasing κ as the filling ratio increases, i.e., $\kappa_{\text{hollow}} > \kappa_{50\%\text{filled}} > \kappa_{100\%\text{filled}}$. Therefore, we assert that thermal transport behaviors in this regime correspond to a well-defined scattering-dominated regime, where guest molecule scattering dominates the dependence of κ on the filling ratio.

In contrast, data below 100 K contradicts the expected trend for phonon transport limited by guest molecule scattering. As depicted in Fig. 2a, below 100 K, the three filling ratios exhibit a non-monotonic trend of $\kappa_{\text{hollow}} > \kappa_{100\%\text{filled}} > \kappa_{50\%\text{filled}}$. This trend is due to the heightened contribution of wavelike coherent phonons to heat conduction at low temperatures, leading to

disorder-dominated thermal transport. In structurally complex materials with many atoms in the unit cell, such as hollow and filled MHs, phase correlation, i.e., coherence of thermal vibrations, is accentuated, particularly at low temperatures, leading to the emergence of wavelike modes, often called "coherent phonons," that transport heat ballistically [37, 38, 39, 40, 41]. Later in this manuscript, we will elucidate this ballistic transport and its contribution to κ using nonequilibrium molecular dynamics (NEMD) simulations.

The 50% filled MH achieves the lowest κ due to its disordered nature, resulting from the random positioning of guest molecules in the cages of the host lattice, unlike the periodic structures of the hollow and 100% filled MHs. This disruption of long-range periodicity in the 50% filled MH suppresses coherent phonon transport through destructive wave interference, greatly reducing κ, particularly at low temperature. This phenomenon is similarly observed in covalent crystals and Lennard-Jones metamaterials featuring secondary periodicity [15, 42, 43, 44, 19, 45]. It is noteworthy that previous studies on clathrate hydrates did not consider the disorder induced by partial filling of guest molecules, thus not capturing the transition between the two thermal transport regimes.

To further validate the transition between the disorder-dominated regime and the scattering-dominated regime, we conduct NEMD simulations of MHs with varying lengths at 50 K and 200 K. As depicted in Fig.2b, at 50 K, MHs of different lengths consistently exhibit a disorder-dominated behavior, with $\kappa_{\text{hollow}} > \kappa_{100\%\text{filled}} > \kappa_{50\%\text{filled}}$. In contrast, at 200 K, all structures demonstrate a scattering-dominated behavior, with $\kappa_{\text{hollow}} > \kappa_{50\%\text{filled}} > \kappa_{100\%\text{filled}}$. These NEMD results align with our EMD data presented in Fig. 2a, reaffirming the existence of two distinct thermal transport regimes. It is noteworthy that the κ of MHs, irrespective of filling ratio, exhibits a notable increase with structure length at 50 K (Fig. 2b), indicating a predominantly ballistic phonon transport resulting from the rather low anharmonic scattering rates at low temperature. Correspondingly, the effect of disorder on κ becomes comparably strong, manifesting as disorder-dominated thermal transport. In contrast, κ, particularly for filled MHs, does not increase much with structure length at 200 K, suggesting

diffusive thermal transport resulting from strong anharmonic scatterings at high temperatures. Correspondingly, the effect of disorder on κ is relatively weaker, thus leading to a monotonic decrease in κ with increasing filling ratio.

To understand the impact of methane guest molecules on the anharmonicity of the host lattice—a factor known to induce a substantial reduction in the κ of certain clathrate structures [9, 10]—we quantify the host lattice's anharmonicity using the methodology recently introduced by Knoop et al.[46]. Given that MH, being a molecular crystal, predominantly conducts heat through the vibrational modes of water molecules within the host lattice, as opposed to the vibrational modes of individual hydrogen or oxygen atoms, we modify Knoop et al.'s approach [46] to align with the molecular-crystal nature of MH. Specifically, our adaptation involves assessing the forces acting on an entire water molecule, rather than an individual atom. This modification is realized by considering the motion of the entire water molecule when evaluating force constants, as opposed to focusing solely on a single atom of interest.

As depicted in Figs. 3a and b, the anharmonic forces F_{anh} acting on water molecules primarily demonstrate a distribution $p(F_{anh})$ within the range of -1 eV/$\mathring{A}$ and 1 eV/$\mathring{A}$, with a notable broadening of $p(F_{anh})$ at higher temperatures. However, it is crucial to note that the broadened $p(F_{anh})$ does not necessarily imply a higher level of anharmonicity. Following Ref. [46], we compute the anharmonicity factor as $\sigma(F_{anh})/\sigma(F)$, where $\sigma(F_{anh})$ and $\sigma(F)$ denote the standard deviations of the anharmonic forces and the total forces, respectively, sampled in our simulations. This ratio provides an environment-independent measure of anharmonicity. As shown in Fig. 3c, the anharmonicity factor remains nearly constant regardless of temperature or filling ratio. This contrasts with prior studies on certain clathrate structures, including $Ba_8Ga_{16}Ge_{30}$ (a semiconductive clathrate) [9], intermetallic clathrates [36], and xenon hydrates [10], where a substantial increase in anharmonicity caused by guest molecules or atoms was observed.

We further analyze spectral phonon properties of hollow and filled MHs using the SED approach. Figure 4 shows the SED contours of filled and hollow

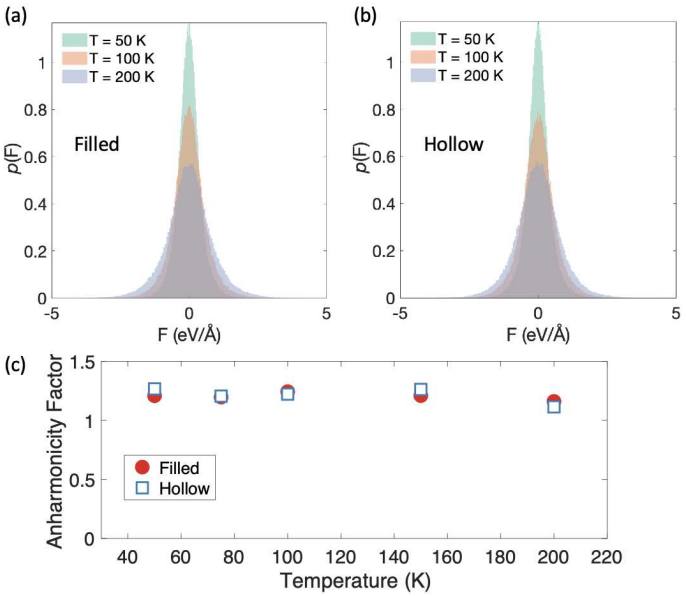

Figure 3: Quantification of anharmonicity in filled and hollow MHs. (a) and (b) display the probability distribution ($p(F)$) of the anharmonic component (F_{anh}) of forces on water molecules. (c) Anharmonic factor as a function of temperature.

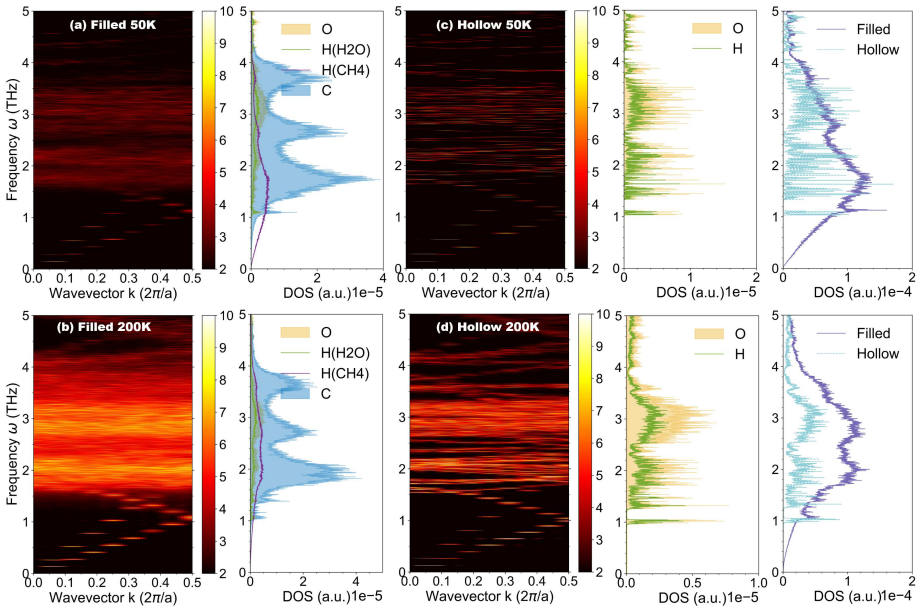

Figure 4: Phonon spectral energy density (logarithmic) plotted in the wavevector-frequency domain for (a) filled MH at 50K, (b) filled MH at 200K, (c) hollow MH at 50K, and (d) hollow MH at 200K. Note that only the 0 Hz - 5 Hz frequency region of the phonon spectrum is plotted, which corresponds to inter-molecule interactions, while the higher-frequency region, which corresponds to intra-molecule interactions, is omitted.

MHs at 50 K and 200 K. Both types of MHs exhibit distinguishable acoustic phonon branches at the temperatures investigated. Since there are respectively 531 and 411 optical phonon branches for filled and hollow MHs, those branches are intertwined in the contour plots. Thus, we will focus on the behaviors of acoustic phonons, which are the primary heat carriers in MHs. Upon comparing Fig. 4a with Fig. 4c, and Fig. 4b with Fig. 4d, it is evident that methane guest molecules do not significantly flatten acoustic bands.

To further validate the absence of band flattening, we present the SED spectra in the frequency domain for hollow and 100% filled MHs at 50 K and 200 K in Figs. 5a-d. For the analysis of phonon lifetime and frequency, we focus on the two lowest-frequency modes. Both filled and hollow MHs exhibit a noticeable reduction in acoustic mode frequencies at higher temperatures due to thermal

expansion. However, the frequencies of the acoustic peaks in filled MH are only slightly lower than those in hollow MH, suggesting a negligible flattening of acoustic bands. This finding contrasts with prior studies on clathrate structures [12], where guests were observed to significantly flatten acoustic bands. However, such disparities are not unexpected, as the impact of guests on the phonon bandstructure of clathrates is influenced by various factors, including the interaction strength between guest and host, the vibrational properties of the guest and host, the relative effective size of the guest molecule compared to the size of the cage, and others [14]. Therefore, the outcome of guest-host interaction necessitates a case-by-case analysis.

Finally, we analyze the influence of methane guest molecules on the lifetime of acoustic phonon modes. As illustrated in Figs. 5b and 5d, and summarized in Fig. 5f, the phonon lifetimes of both filled and hollow MHs decrease notably at elevated temperatures, attributed to intensified anharmonic phonon scattering. This explains the notable reduction in κ of both MH structures as the temperature rises, as displayed in Fig. 2. Moreover, filled MHs exhibit shorter phonon lifetimes than their hollow counterparts, further confirming the adverse impact of guest molecules on phonon lifetimes and thus κ.

Figure 4 presents the vibrational density of states (DOS) of various types of atoms in MH. The DOS of carbon and hydrogen atoms within methane overlap significantly with the acoustic phonon bands in the SED contours, supporting the guest molecule scattering theory of clathrate structures. Notably, a substantial portion of DOS below 1 THz is observed in methane molecules, attributed to their ability to move within the water cage. In contrast, water molecules exhibit considerably lower vibrational energy below 1 THz due to their constrained motion within the host lattice. Additionally, the introduction of methane molecules to an initially hollow MH is expected to increase the anharmonic phonon-phonon scattering phase space for acoustic phonons. However, we assert that this is a secondary effect, as the original scattering phase space is already large due to the presence of a significant number of closely positioned optical branches, as depicted in the SED contours of Fig. 4.

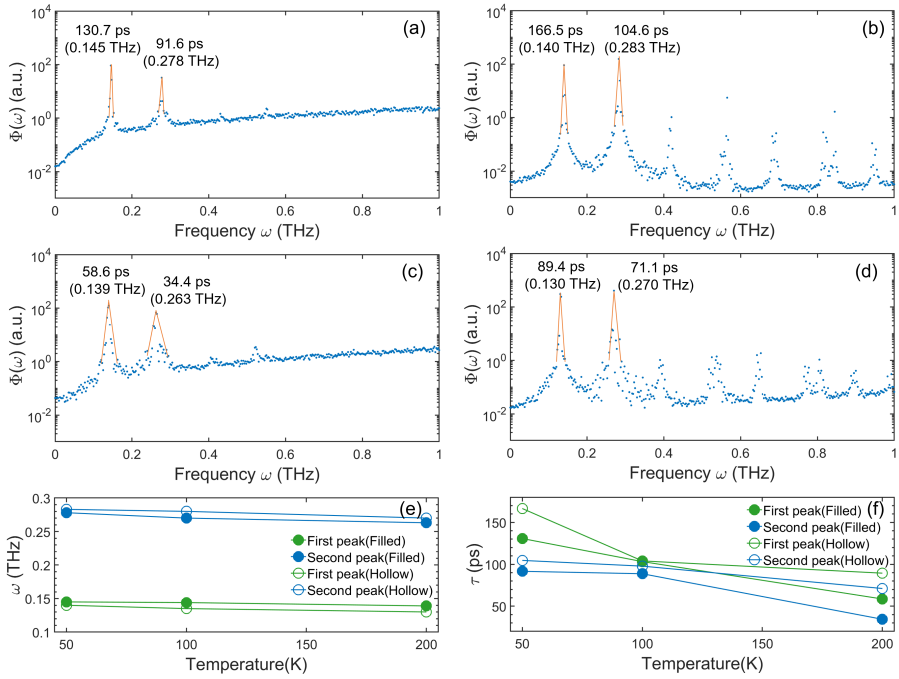

Figure 5: SED as a function of phonon frequency at wavevector $k = 0.05$ (reduced coordinates) along the [1 0 0] direction of the reciprocal space for (a) filled MH at 50K, (b) hollow MH at 50K, (c) filled MH at 200K, and (d) hollow MH at 200K. (e) Temperature-dependent acoustic phonon frequency. (f) Temperature-dependent phonon lifetime.

4. Conclusion

In summary, we developed a high-accuracy DNN interatomic potential for type-I MH through AIMD simulations. Leveraging this potential, our MD simulations provided insights into the κ of hollow, partially filled, and 100% filled MHs. Notably, our investigation revealed two distinctive thermal transport regimes, i.e., disorder-dominated and scattering-dominated, in partially filled MHs, a prevalent configuration in real-world MHs. Above 100 K, thermal transport is mainly constrained by guest molecule scattering and intrinsic anharmonic processes, while below 100 K, disorder in guest molecules becomes a significant factor, leading to a notable reduction in κ. Importantly, our study refutes the notion that methane guest molecules induce elevated anharmonicity or flatten acoustic bands in the host lattice. Instead, we demonstrate that these molecules directly scatter host lattice phonons, which is the primary mechanism for the lower κ of filled MHs than their hollow counterparts. Our findings underscore the critical role of structural disorder on thermal transport in MHs and furnish detailed insights into the intricate influence of guest molecules on the thermal transport properties of MHs, which holds substantial importance for the comprehensive exploration and exploitation of this noteworthy energy resource.

Author Contributions

Rajan, Cui, and Maranets made equal contributions to this work. Rajan conducted AIMD simulations and played a key role in training the DNN interatomic potential. Cui carried out EMD simulations and performed SED analyses. Maranets conducted NEMD simulations. Wang supervised the project. All authors contributed to the conceptualization of the research and actively participated in the analysis and discussion of the results, as well as contributing to the writing of the manuscript.

Acknowledgement

Acknowledgment is made to the donors of the American Chemical Society Petroleum Research Fund (60587-DNI10) for support of this research. T.M. thanks the support from the National Science Foundation (award number: 2047109).

Data Availability Statement

The data that support the findings of this study are available from the corresponding author, Y. W., upon reasonable request.

References

[1] K. A. Kvenvolden, Methane hydrate—a major reservoir of carbon in the shallow geosphere?, Chemical geology 71 (1-3) (1988) 41–51.

[2] B. Buffett, D. Archer, Global inventory of methane clathrate: sensitivity to changes in the deep ocean, Earth and Planetary Science Letters 227 (3-4) (2004) 185–199.

[3] R. Ross, P. Andersson, G. Bäckström, Unusual pt dependence of thermal conductivity for a clathrate hydrate, Nature 290 (5804) (1981) 322–323.

[4] P. Andersson, R. Ross, Effect of guest molecule size on the thermal conductivity and heat capacity of clathrate hydrates, Journal of Physics C: Solid State Physics 16 (8) (1983) 1423.

[5] J. S. Tse, M. A. White, Origin of glassy crystalline behavior in the thermal properties of clathrate hydrates: a thermal conductivity study of tetrahydrofuran hydrate, The Journal of Physical Chemistry 92 (17) (1988) 5006–5011.

[6] A. Krivchikov, B. Y. Gorodilov, O. Korolyuk, V. Manzhelii, O. Romantsova, H. Conrad, W. Press, J. Tse, D. Klug, Thermal conductivity of xe clathrate hydrate at low temperatures, Physical Review B 73 (6) (2006) 064203.

[7] W. F. Waite, L. A. Stern, S. Kirby, W. J. Winters, D. Mason, Simultaneous determination of thermal conductivity, thermal diffusivity and specific heat in si methane hydrate, Geophysical journal international 169 (2) (2007) 767–774.

[8] N. J. English, J. S. Tse, Perspectives on hydrate thermal conductivity, Energies 3 (12) (2010) 1934–1942.

[9] T. Tadano, Y. Gohda, S. Tsuneyuki, Impact of rattlers on thermal conductivity of a thermoelectric clathrate: a first-principles study, Physical review letters 114 (9) (2015) 095501.

[10] C. Yuan, Z. Zhang, J. Zhu, J. Zhao, L. Zhang, L. Yang, Y. Song, D. Tang, Heat transport in clathrate hydrates controlled by guest frequency and host–guest interaction, The Journal of Physical Chemistry Letters 14 (34) (2023) 7766–7772.

[11] G. A. Slack, V. G. Tsoukala, Some properties of semiconducting irsb3, Journal of Applied Physics 76 (3) (1994) 1665–1671.

[12] M. Christensen, A. B. Abrahamsen, N. B. Christensen, F. Juranyi, N. H. Andersen, K. Lefmann, J. Andreasson, C. R. Bahl, B. B. Iversen, Avoided crossing of rattler modes in thermoelectric materials, Nature materials 7 (10) (2008) 811–815.

[13] C. Lee, A. Nishida, T. Hasegawa, H. Nishiate, H. Kunioka, S. Ohira-Kawamura, M. Nakamura, K. Nakajima, Y. Mizuguchi, Effect of rattling motion without cage structure on lattice thermal conductivity in laobis2-xsex, Applied Physics Letters 112 (2) (2018).

[14] S. Pailhès, H. Euchner, V. M. Giordano, R. Debord, A. Assy, S. Gomès, A. Bosak, D. Machon, S. Paschen, M. De Boissieu, Localization of propagative phonons in a perfectly crystalline solid, Physical review letters 113 (2) (2014) 025506.

[15] Y. Wang, H. Huang, X. Ruan, Decomposition of coherent and incoherent phonon conduction in superlattices and random multilayers, Phys. Rev. B 90 (2014) 165406. doi:10.1103/PhysRevB.90.165406.
URL https://link.aps.org/doi/10.1103/PhysRevB.90.165406

[16] T. Ma, C.-T. Lin, Y. Wang, The dimensionality effect on phonon localization in graphene/hexagonal boron nitride superlattices, 2D Materials 7 (3) (2020) 035029.

[17] P. Chakraborty, Y. Liu, T. Ma, X. Guo, L. Cao, R. Hu, Y. Wang, Quenching thermal transport in aperiodic superlattices: a molecular dynamics and machine learning study, ACS applied materials & interfaces 12 (7) (2020) 8795–8804.

[18] Y. Liu, R. Hu, Y. Wang, J. Ma, Z. Yang, X. Luo, Big-data-accelerated aperiodic si/ge superlattice prediction for quenching thermal conduction via pattern analysis, Energy and AI 3 (2021) 100046. doi:https://doi.org/10.1016/j.egyai.2020.100046.
URL https://www.sciencedirect.com/science/article/pii/S266654682030046X

[19] T. Maranets, M. Nasiri, Y. Wang, Influence of spatial coherence on phonon transmission across aperiodically arranged interfaces, Physics Letters A (2024) 129572.

[20] Ab initio molecular dynamics for liquid metals, Physical review B 47 (1) (1993) 558.

[21] G. Kresse, J. Furthmüller, Efficiency of ab-initio total energy calculations for metals and semiconductors using a plane-wave basis set, Computational materials science 6 (1) (1996) 15–50.

[22] H. Wang, L. Zhang, J. Han, E. Weinan, Deepmd-kit: A deep learning package for many-body potential energy representation and molecular dynamics, Computer Physics Communications 228 (2018) 178–184.

[23] Y. Zhang, H. Wang, W. Chen, J. Zeng, L. Zhang, H. Wang, E. Weinan, Dp-gen: A concurrent learning platform for the generation of reliable deep learning based potential energy models, Computer Physics Communications 253 (2020) 107206.

[24] A. P. Thompson, H. M. Aktulga, R. Berger, D. S. Bolintineanu, W. M. Brown, P. S. Crozier, P. J. in't Veld, A. Kohlmeyer, S. G. Moore, T. D. Nguyen, et al., Lammps-a flexible simulation tool for particle-based materials modeling at the atomic, meso, and continuum scales, Computer Physics Communications 271 (2022) 108171.

[25] S. Nosé, A unified formulation of the constant temperature molecular dynamics methods, The Journal of chemical physics 81 (1) (1984) 511–519.

[26] W. G. Hoover, Canonical dynamics: Equilibrium phase-space distributions, Physical review A 31 (3) (1985) 1695.

[27] Y. Wang, C. Gu, X. Ruan, Optimization of the random multilayer structure to break the random-alloy limit of thermal conductivity, Applied Physics Letters 106 (7) (2015).

[28] M. S. Green, Markoff random processes and the statistical mechanics of time-dependent phenomena. ii. irreversible processes in fluids, The Journal of chemical physics 22 (3) (1954) 398–413.

[29] R. Kubo, Statistical-mechanical theory of irreversible processes. i. general theory and simple applications to magnetic and conduction problems, Journal of the physical society of Japan 12 (6) (1957) 570–586.

[30] T. Schneider, E. Stoll, Molecular-dynamics study of a three-dimensional one-component model for distortive phase transitions, Physical Review B 17 (3) (1978) 1302.

[31] T. Maranets, H. Cui, Y. Wang, Lattice thermal conductivity of embedded nanoparticle composites: the role of particle size distribution, Nanotechnology 35 (5) (2023) 055701.

[32] J. A. Thomas, R. M. Iutzi, A. J. H. McGaughey, Thermal conductivity and phonon transport in empty and water-filled carbon nanotubes, Phys. Rev. B 81 (2010) 045413. doi:10.1103/PhysRevB.81.045413.
URL https://link.aps.org/doi/10.1103/PhysRevB.81.045413

[33] T. Feng, B. Qiu, X. Ruan, Anharmonicity and necessity of phonon eigenvectors in the phonon normal mode analysis, Journal of Applied Physics 117 (19) (2015) 195102. doi:10.1063/1.4921108.
URL https://doi.org/10.1063/1.4921108

[34] T. Ma, P. Chakraborty, X. Guo, L. Cao, Y. Wang, First-principles modeling of thermal transport in materials: Achievements, opportunities, and challenges, International Journal of Thermophysics 41 (2020) 1–37.

[35] R. Pohl, Thermal conductivity and phonon resonance scattering, Physical review letters 8 (12) (1962) 481.

[36] M. Beekman, A. VanderGraaff, High-temperature thermal conductivity of thermoelectric clathrates, Journal of Applied Physics 121 (20) (2017).

[37] B. Latour, Y. Chalopin, Distinguishing between spatial coherence and temporal coherence of phonons, Physical Review B 95 (21) (2017) 214310.

[38] M. Simoncelli, N. Marzari, F. Mauri, Unified theory of thermal transport in crystals and glasses, Nature Physics 15 (8) (2019) 809–813.

[39] Z. Zhang, Y. Guo, M. Bescond, J. Chen, M. Nomura, S. Volz, Generalized decay law for particlelike and wavelike thermal phonons, Physical Review B 103 (18) (2021) 184307.

[40] Z. Zhang, Y. Guo, M. Bescond, J. Chen, M. Nomura, S. Volz, Heat conduction theory including phonon coherence, Physical Review Letters 128 (1) (2022) 015901.

[41] Z. Zhang, Y. Guo, M. Bescond, J. Chen, M. Nomura, S. Volz, How coherence is governing diffuson heat transfer in amorphous solids, npj Computational Materials 8 (1) (2022) 96.

[42] M. N. Luckyanova, J. Mendoza, H. Lu, B. Song, S. Huang, J. Zhou, M. Li, Y. Dong, H. Zhou, J. Garlow, L. Wu, B. J. Kirby, A. J. Grutter, A. A. Puretzky, Y. Zhu, M. S. Dresselhaus, A. Gossard, G. Chen, Phonon localization in heat conduction, Science Advances 4 (12) (2018) eaat9460. arXiv:https://www.science.org/doi/pdf/10.1126/sciadv.aat9460, doi:10.1126/sciadv.aat9460.
URL https://www.science.org/doi/abs/10.1126/sciadv.aat9460

[43] P. Chakraborty, L. Cao, Y. Wang, Ultralow lattice thermal conductivity of the random multilayer structure with lattice imperfections, Scientific Reports 7 (1) (2017) 8134. doi:10.1038/s41598-017-08359-2.
URL https://doi.org/10.1038/s41598-017-08359-2

[44] P. Chakraborty, I. A. Chiu, T. Ma, Y. Wang, Complex temperature dependence of coherent and incoherent lattice thermal transport in superlattices, Nanotechnology 32 (6) (2020) 065401.

[45] T. Maranets, Y. Wang, Prominent phonon transmission across aperiodic superlattice through coherent mode-conversion (2024). arXiv:2405.18647.

[46] F. Knoop, T. A. R. Purcell, M. Scheffler, C. Carbogno, Anharmonicity measure for materials, Phys. Rev. Mater. 4 (2020) 083809. doi:10.1103/PhysRevMaterials.4.083809.
URL https://link.aps.org/doi/10.1103/PhysRevMaterials.4.083809